Contents lists available at ScienceDirect

# **Extreme Mechanics Letters**

journal homepage: www.elsevier.com/locate/eml



# Tunable tensile response of honeycomb plates with nanoscale thickness: Testing and modeling



Pengcheng Jiao <sup>a,\*</sup>, Samuel M. Nicaise <sup>b</sup>, Mohsen Azadi <sup>b</sup>, Joan Cortes <sup>b</sup>, Drew E. Lilley <sup>b</sup>, Wujoon Cha <sup>b</sup>, Prashant K. Purohit <sup>b</sup>, Igor Bargatin <sup>b,\*</sup>

- <sup>a</sup> Ocean College, Zhejiang University, Zhoushan 316021, Zhejiang, China
- b Department of Mechanical Engineering and Applied Mechanics, University of Pennsylvania, Philadelphia, PA 19104, USA

### ARTICLE INFO

Article history:
Received 20 August 2019
Received in revised form 1 November 2019
Accepted 6 November 2019
Available online 13 November 2019

Keywords:
Mechanical metamaterials
Tunable tensile response
Honeycomb plates
Theoretical modeling
Nanoscale fabrication and experiment
Numerical simulation

#### ABSTRACT

Plate mechanical metamaterials with nanoscale thickness demonstrate significantly enhanced mechanical properties compared to solid plates that lack micropatterning. We have previously reported how the honeycomb corrugation greatly increases the bending stiffness, but any functional applications also require a full understanding of the tensile properties. Here we report that, surprisingly, the tensile properties of alumina plates with nanoscale thickness can be measured using conventional materials testing tools and that the tensile stiffness of honeycomb corrugated plates is greatly reduced, providing an unusual combination of high bending stiffness and low tensile stiffness that cannot be achieved with unpatterned plates. These measurements, along with finite-element (FE) simulations, provide validation for our analytical model that fully characterizes the tensile response of the corrugated nanoplates, thus enabling predictable tuning of their mechanical properties by changing the corrugation geometry. Plates optimized for high bending stiffness and low tensile stiffness can find applications as wings of microflyers or deployable aerospace components.

© 2019 Elsevier Ltd. All rights reserved.

## 1. Introduction

Flat plates, such as plywood, paper, and glass sheets, are frequently used as structural components but, for cutting-edge miniaturized applications such as robotic microflyers, structural plates need to be ultralight and therefore ultrathin. For example, Fig. 1(a) illustrates the concept of a next-generation microflyer that would need to be constructed out of plates that are both strong and ultralight. Another potential application is using ultralight weight plates to construct lightsails that could one day propel an interstellar probe to Alpha Centauri [1]. In this case, the areal density of the sail should be 1 gm<sup>-2</sup> or less and the plates must be adequately stiff to support complex loading, yet also flexible enough to not break under large deformations caused by collisions or stowing.

One way to achieve such ultralight wings is to reduce the plate thickness to well below 1 micrometer. In practice, however, such thin, planar films possess extremely low bending stiffness and, therefore, can easily fold and stick to themselves. To enhance the mechanical performance of thin, lightweight structural materials, many mechanical metamaterials have been investigated

in recent years [2–6]. Studies have been mainly focused on 3D bulk mechanical metamaterials under different loading conditions, e.g., compression [7–10], tension [11–13], or rotation [14]. Origami and kirigami have also been investigated to create complex 3D structures from 2D sheets by out-of-plane deformations through folding or folding with cutting [15–17]. Few-layer bismuthene and MXene have also been reported with unique electronic and mechanical characteristics [18–20]. However, only a few studies have been conducted on plate-like structures that would be most relevant to robotic wings, lightsails, and similar applications.

To address the lack of research, we recently introduced ultralight plate mechanical metamaterials that use micro-corrugated webbing to enhance mechanical performance [21–23]. Experimentally, metamaterial plates with  $\sim \text{cm}^2$  area and  $\sim \text{nm}$  thickness were stiff enough to not sag under their own weight, and completely recovered their shape after large deformation in bending. They provide an example of a plate material that is ultralight, as well as stiff and robust enough to be considered as a structural component at the macroscopic scale. Our previous work focused primarily on the bending and shear properties [21,22,24,25]. However, for most miniature applications, the nanoplates would be subjected to more complex loading involving not only bending, but also stretching, as shown in Fig. 1(b). Thus, the tensile properties of the corrugated nanoplates

<sup>\*</sup> Corresponding authors.

E-mail addresses: pjiao@zju.edu.cn (P. Jiao), bargatin@seas.upenn.edu

I. Bargatin).

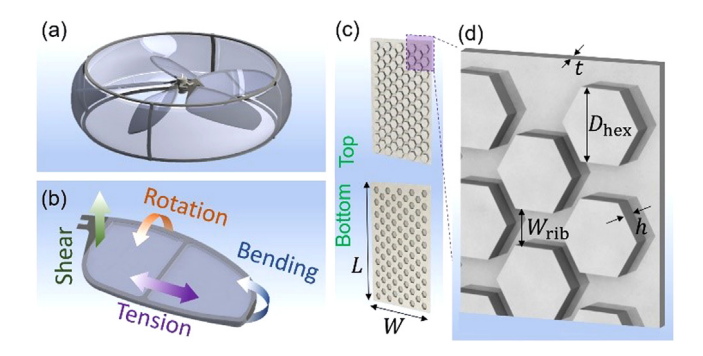


**Fig. 1.** (a) Illustration of next-generation microflyers with microscale wings. (b) Deformations of the wing membranes — combination of bending, twisting and stretching. (c) Nanoscale plates with hexagonal corrugations that have low tensile stiffness and enhanced bending stiffness. (d) Illustration of the parameters of the hexagonal designs: diameter $D_{hex}$ , rib width  $W_{rib}$ , thickness t, and height h.

must be considered in order to predict performance and prevent failure.

In this letter, we complete the mechanical characterization of the corrugated nanoplates by investigating the tensile response. We experimentally characterized the tensile response of our alumina nanoscale plates using a standard material testing system and procedure. The tensile modulus of uncorrugated planar alumina nanofilms was also validated, providing a baseline for the corrugated nanoplates. Analytical and numerical models of corrugated nanoplates were then developed, and the predictions were compared to the experimental observations.

The effective tensile Young's modulus of the architected plates was studied with respect to the geometric parameters in Figs. 1(c) and (d) (i.e., height h, thickness t, hexagonal diameter  $D_{hex}$ , and rib width  $W_{rib}$ ). In combination with our previous studies on bending, this letter highlights geometric optimization for reduced tensile resistance and increased bending resistance with respect to a minimum body weight. The tunable mechanical behavior makes the nanoplates appropriate for applications in lightsails [1], wearables [26], wings for microrobots [27,28], and piezoelectric nanogenerators (PENG) [29]. We particularly envision the reported plates as a sensing platform for biochemical applications [30] or skin-like technology in health care [31]. Taking advantage of the honeycomb corrugation, the nanoplates can provide an adjustable mechanical response while the hexagonal cells provide storage and protection to sensitive electric microdevices, biological cells, or other microscopic objects in specific applications.

#### 2. Experimental setup, nanoscale fabrication and testing

Fig. 2 illustrates the studied nanoplates, as well as the experimental setup for tensile testing and finite element (FE) modeling. Fig. 2(a) shows the nanoscale alumina cantilevered plates with hexagonal corrugation, with previous reports providing more indepth coverage of the materials and fabrication process [21,22] (Sec. 1 in the supplemental material). We chose a hexagonal geometry because it is an approximately isotropic arrangement that mimics many natural nanoscale materials [32–34]. To benchmark the changes in the mechanical response due to the corrugation, we also experimentally measured the tensile stiffness of planar, uncorrugated nanofilms, as shown in Fig. 2(b), to be  $E_{\rm s} \approx$  120 GPa. To support these otherwise floppy planar nanoscale films, we surrounded them with corrugated nanoplates, which prevented the planar films from folding onto themselves but contributed only negligibly to the measured tensile stiffness. Fig. 2(c)

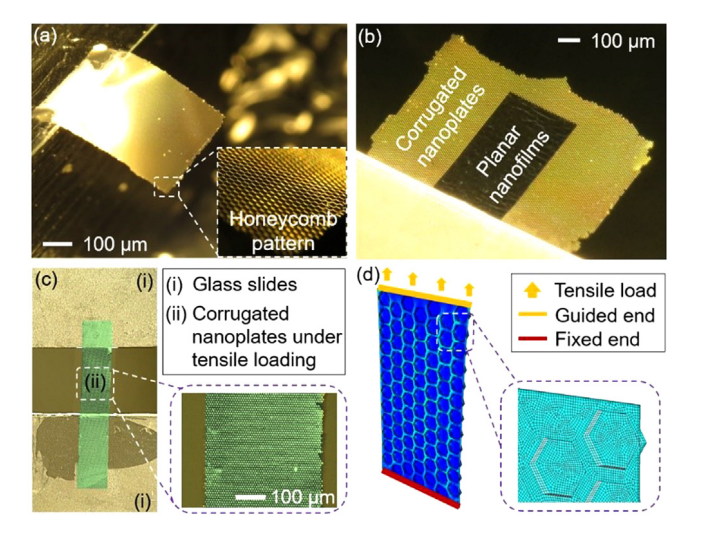


**Fig. 2.** (a) Nanoscale cantilevered plates with honeycomb corrugation. (b) Experimental calibration of the tensile stiffness of uncorrugated alumina planar nanofilms that have the same length, width and thickness as the nanoplates. (c) Experimental setup and tensile testing of the corrugated nanoplates using Instron loading machine. (d) FE modeling of the nanostructures under axial tension ( $L=1\,$  mm,  $W=0.5\,$  mm,  $h=10\,$  μm,  $D_{hex}=50\,$  μm,  $W_{rib}=10\,$  μm, and  $t=400\,$  nm).

shows the experimental setup of the tensile testing using the materials tester in which the plates were epoxied to two glass slides which were themselves attached to the testing fixture. Fig. 2(d) shows an example of the FE models built in Abaqus 2017x (Sec. 2 in the supplemental material). The S4R shell element in ABAQUS was used to simulate the thin nature of the corrugated plates. Clamped-guided boundary conditions were used for the plates.

# 3. Theoretical Modeling of the Corrugated Nanoplates Subjected to Tension

To explain the experimental observations and FE simulation, we also analytically modeled the architected nanostructures (Sec. 3 in the supplemental material). Fig. 3(a) presents the deformation analysis of an arbitrary corrugation cell in the axial tension. A key observation in this regard is that the majority of deformation occurs (as in Fig. S8(a)) in the channels. At the same time, the planar hexagons do have much effect on the tensile stiffness except by preventing in-plane Poisson contraction that is perpendicular to the tensile loading [35]. Hence, our strategy is to compute the in-plane moduli of the honeycomb structure under the constraint that no Poisson contraction occurs. The work done by the axial force F is stored as elastic energy in the honeycomb, hence we equate the work to the bending and twisting energy in the channel cross-section struts as [36]

$$F\delta = \alpha' \frac{E_{\rm s} I \delta^2}{D_{\rm hex}^3} + \beta' \frac{E_{\rm s} h^4 W_{\rm rib}^4 \delta^2}{t D_{\rm hex}^5 (W_{\rm rib} + 2h)},$$
 (1)

where  $\alpha'$  and  $\beta'$  are the constants that characterize the bending and twisting mechanisms of the nanoplates, respectively.  $\delta$  and I, the deflection and moment of inertia, are given as

$$\begin{cases} \delta = \frac{\sqrt{3}FD_{\text{hex}}^3}{3E_5I} \\ I = \frac{tW_{\text{rib}}^3}{12} + \frac{t^3h}{6} + \frac{thW_{\text{rib}}^2}{2}. \end{cases}$$
 (2)

Note that symbol nomenclature in the theoretical model is summarized in Table S3 in the supplemental material.

Since the effective Young's modulus of the nanoplates  $E^*$  is proportional to  $\frac{F}{\delta}$ , Eq. (1) can be rewritten as the ratio of the

Young's moduli between the corrugated nanoplates and planar nanofilms:

$$\frac{E^*}{E_s} = \alpha \frac{I}{tW_{\text{rib}}^3} + \beta \frac{h^4 W_{\text{rib}}^4}{t^2 D_{\text{hex}}^5 (W_{\text{rib}} + 2h)},$$
(3)

where  $\alpha$  and  $\beta$  are the constants based on  $\alpha'$  and  $\beta'$ . We fitted the numerical simulation results of  $\frac{E^*}{E_S}$  using the nonlinear least-squares algorithm for a variety of different geometric parameters, with the best fit corresponding to  $\alpha=0.234$  and  $\beta=0.062$ . Assuming the force F acts through the centroid of the channel section, Eq. (3) is rewritten as

$$E^* = E_{\rm s} \left[ \alpha \frac{I}{t D_{\rm hex}^3} + \beta \frac{\Psi}{t^4 D_{\rm hex}^5 (2h + W_{\rm rib})} \right], \tag{4}$$

where 
$$\Psi = \left(\frac{th^2W_{\rm rib}^2}{4} + \frac{I}{2} \cdot \frac{2h^2 + tW_{\rm rib}}{2h + W_{\rm rib}}\right)^2$$
. Further assuming the

honeycomb to be an elastic continuum under plane-stress, the effective Young's modulus of the honeycomb corrugated plates in the longitudinal direction can be characterized as

$$E_{11}^* = \frac{\sigma_{11}}{\varepsilon_{11}} = \frac{E^*}{1 - v^{*2}},\tag{5}$$

and the effective Poisson's ratio is given as

$$v^* = \frac{\Lambda - 36I}{\Lambda + 108I},\tag{6}$$

where  $\Lambda = AD_{\rm hex}^2 + 3 (2.4 + 1.5 \nu_{\rm s}) AW_{\rm rib}^2$ . Note that  $A = t (2h + W_{\rm rib})$  denotes the cross-sectional area of the channel in Fig. 3(a), and  $\nu_{\rm s}$  is the Poisson's ratio of the alumina nanofilms. Note that bending, shear and stretching deformations are considered in the hexagonal struts for the Poisson's ratio; however, stretching is not considered in the tensile modulus.

Substituting Eq. (4) into Eq. (5), the effective Young's modulus of the corrugated nanoplates in the longitudinal direction is obtained as

$$E_{11}^* = \frac{E_{\rm s}}{1 - \left(\frac{A - 36I}{A + 108I}\right)^2} \left[ \frac{0.234I}{tD_{\rm hex}^3} + \frac{0.062\Phi}{t^4 D_{\rm hex}^5 (2h + W_{\rm rib})} \right]. \tag{7}$$

Figs. 3(b) and (c) compare the tensile stress–strain relations of the corrugated nanoplates between the experimental, numerical and analytical results based on Eq. (7), and good agreements are obtained between  $E_{\text{num}}^*$ ,  $E_{\text{exp}}^*$  and  $E_{\text{theo}}^*$  from both the comparisons.

# 4. Parametric studies

# 4.1. Optimal effect regions (OERs)

To study the tunability of the tensile stiffness (the slope of the force–displacement curves), we define the stiffness ratio between the corrugated plates and planar films  $\frac{K_{\rm cp}}{K_{\rm pf}}$ , which we call tensile stiffness reduction factor *TSRF*, as (Sec. 4 in the supplemental material)

$$TSRF = \frac{K_{cp}}{K_{pf}} = \frac{h}{t} \frac{E_{11}^*}{E_s},$$
 (8)

where  $K_{\rm cp}$  and  $K_{\rm pf}$  denote the tensile stiffnesses of the corrugated plates and planar films, respectively. Fig. 4(a) shows the density plot of  $TSRF_{\rm hex}$  for hexagonal nanoplates obtained using the analytical model, and Fig. 4(b) presents the numerical results. Note that  $TSRF_{\rm hex}$  is studied with respect to the pattern ratio of diameter-to-rib width  $\frac{D_{\rm hex}}{W_{\rm rib}}$  and geometric ratio of height-to-thickness  $\frac{h}{t}$ . Satisfactory agreements of the patterns are obtained between the analytical and numerical predictions. Based on our previous studies on the corrugated plates in compression, the

bending stiffness enhancement factor can be written with the pattern ratio as  $BSEF_{\rm hex} \approx \left(\frac{D_{\rm hex}}{W_{\rm rib}}+1\right)^2$  [21]. Fig. 4(c) presents the optimal effect region (OER) for the corrugated plates comparing with the planar films. We can see that the optimal geometries that lead to high bending stiffness (i.e.,  $BSEF_{\rm hex} > 125$ ) and low tensile stiffness (i.e.,  $TSRF_{\rm hex} < 0.05$ ) are achieved with smaller  $\frac{h}{t}$  and larger  $\frac{D_{\rm hex}}{W_{\rm rib}}$ . In order to better characterize the bending and tensile relationship, we also investigated the  $BSEF_{\rm hex}$ -to- $TSRF_{\rm hex}$  ratio, which can be viewed as a figure of merit of the plate metamaterials that simultaneously have high bending stiffness and low tensile stiffness (Fig. 4(d)). In solid plates, including the planar nanofilms in Fig. 2(b), the tensile and stiffness increase together with increasing thickness and this ratio is always one. In our plate metamaterials, this figure-of-merit ratio can exceed several thousand for geometries with high  $\frac{D_{\rm hex}}{W_{\rm rib}}$  and low  $\frac{h}{t}$  (Fig. 4(d)).

The honeycomb corrugation investigated in this letter can be expanded to other patterns. We defined two design rules for the architected metamaterial plates (i.e., the no-straight-line rule and regularity rule) and investigated alternative corrugation patterns (Sec. 5.1 in the supplemental material). Rhombille, basketweave and cylindrical patterns were numerically investigated to obtain the regions of TSRF and BSEF, as shown in Fig. 5. Compared to  $\frac{h}{r}$ , the diameter-to-rib width ratio is likely to affect the TSRF and BSEF more significantly. This indicates that the corrugation patterns can be used to efficiently tune the bending and tensile responses of the nanoplates, while maintaining their overall geometries (e.g., length, width, thickness or height) the same. It can be seen from Fig. 5 that when the thickness t and pattern-specific rib width  $W_{\text{pat}}$  are fixed as constants, smaller nanoplates height h and larger pattern-specific unit diameter  $D_{pat}$  are likely to provide the optimal effects in both bending and tension. The BSEF<sub>pat</sub>to-TSRF<sub>pat</sub> ratios for the rhombille, basketweave and cylindrical corrugations are given in Sec. 5.2 in the supplemental material

#### 4.2. Areal density ratios

To obtain the optimal design ratios  $\frac{h}{t}$  and  $\frac{D_{\text{pat}}}{W_{\text{pat}}}$  that lead to the minimum self-weight, we further analyzed the areal density of the nanoplates. In particular, the ratio of the corrugated plate areal density to that of planar film  $\frac{AD_{\text{cp}}}{AD_{\text{pf}}}$  was used to compare between the hexagonal, rhombille, basketweave and cylindrical nanoplates, as shown in Fig. 6. The obtained optimal effect regions (OERs) from Figs. 4(c) and 5 are shaded. We found that no other patterns offer significantly better performance than the hexagonal corrugation in Fig. 6(a).

We note that, in principle, the same mechanical response can be obtained at larger length scales as long as  $\frac{h}{t}$  and  $\frac{D_{\text{hex}}}{W_{\text{rib}}}$  are maintained the same. However, the reported nanoplates have extremely large aspect ratio (i.e., height-to-thickness ratio is  $\sim 10^3$ ), making it difficult to manufacture and test similar plates at the macroscale. To maintain the unique mechanical response of the corrugated plates with  $\sim 100~\mu\text{m}$  such as with paper thickness, the height h needs to be scaled up to the meter-scale, which requires the length L and width W to be at the scale of tens or hundreds of meters.

#### 5. Conclusions

In this letter, we presented nanoscale plates with corrugated patterns that have high bending stiffness in combination with low tensile stiffness. Nanofabrication was used to manufacture the honeycomb nanoplates and planar nanofilms. Surprisingly, experimental testing could be carried out using a standard material tester to obtain the effective Young's moduli of the nanoplates  $E_{11}^*$ 

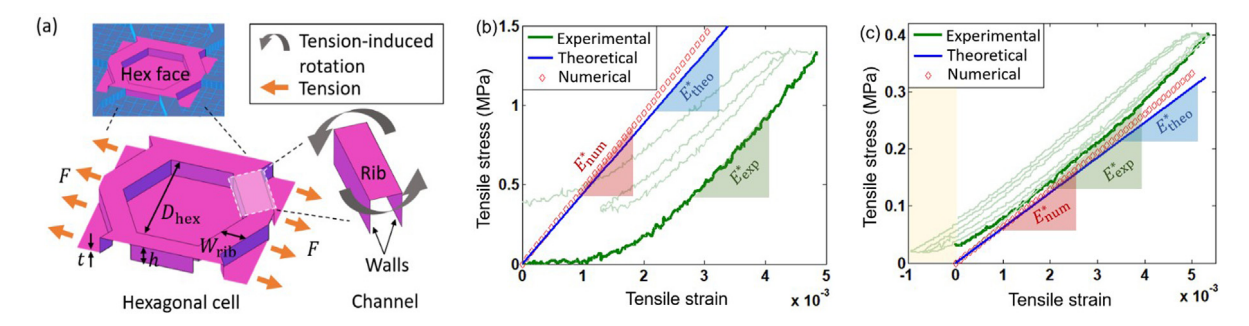


**Fig. 3.** (a) Deformation illustration of an axially loaded honeycomb cell in the nanoplates. Comparisons of the effective Young's moduli between the experimental, analytical and FE results for (b) L=6 mm, W=3 mm, t=400nm, and (c) L=4 mm, W=8 mm, t=100 nm, (h=10  $\mu$ m,  $D_{hex}=50$   $\mu$ m and  $W_{rib}=10$   $\mu$ m for both of the cases). The experimental curves show hysteresis but the slope (stiffness) remains consistent throughout the measurements.

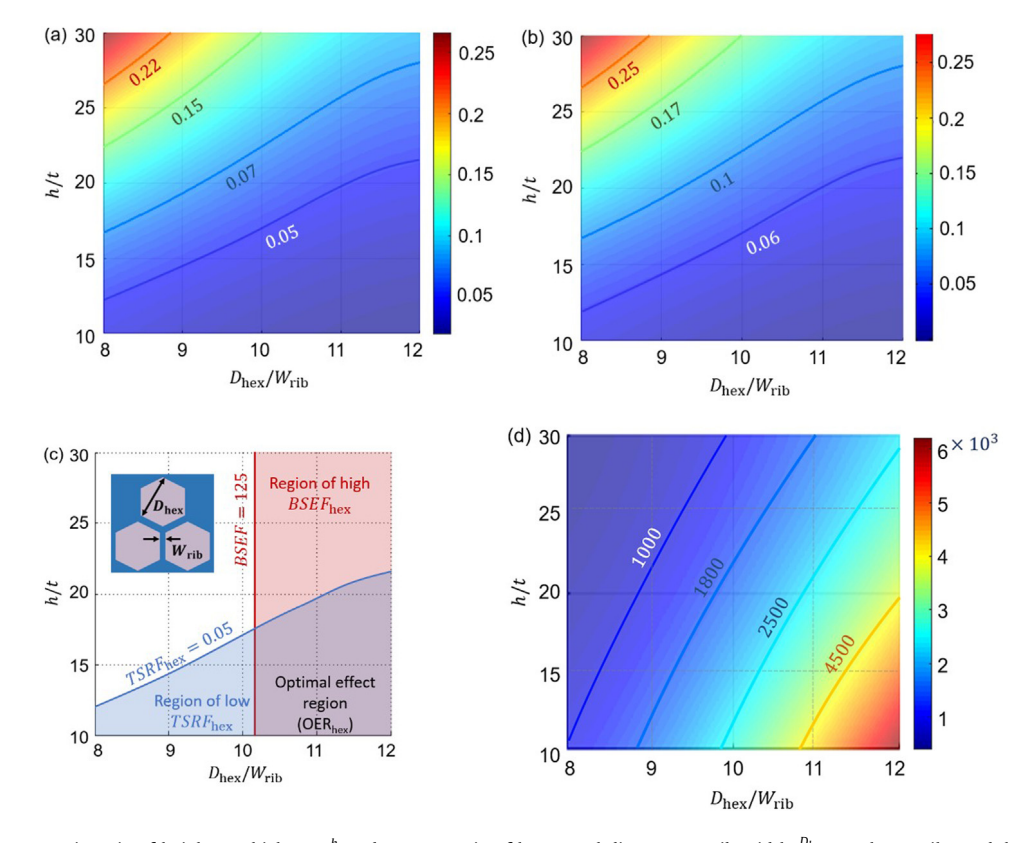
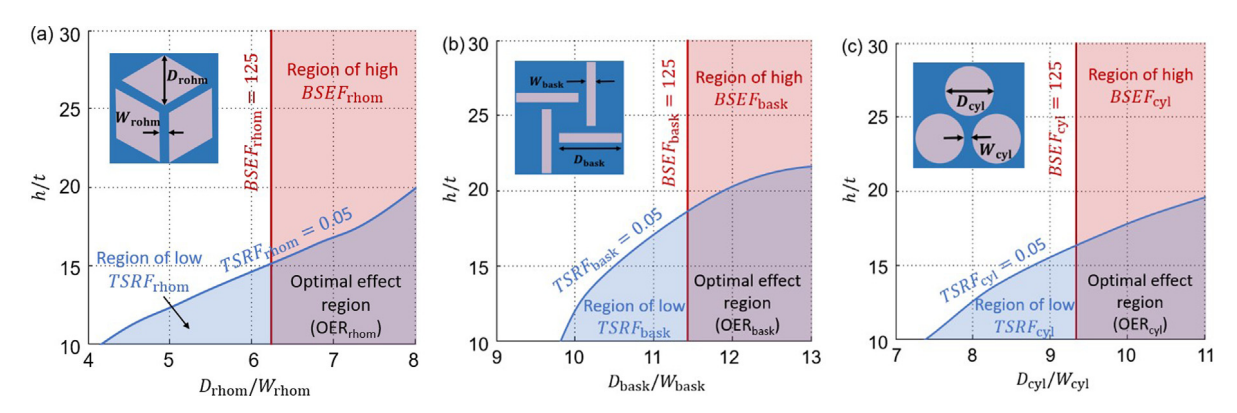
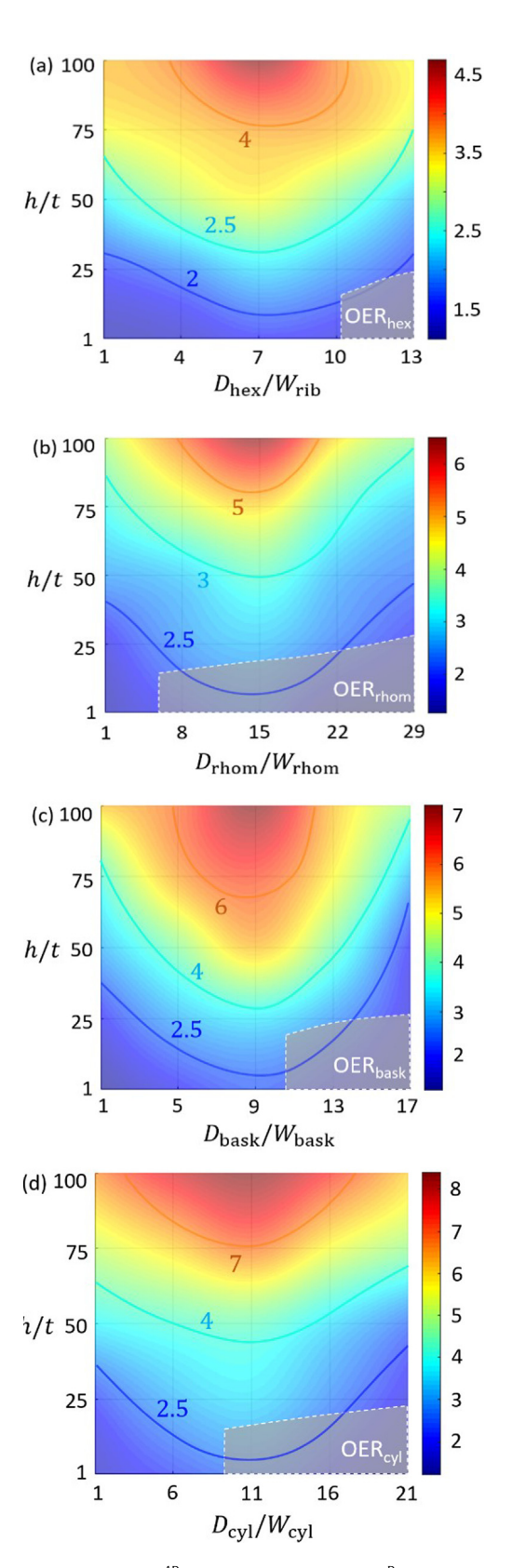


Fig. 4. Effects of the geometric ratio of height-to-thickness  $\frac{h}{t}$  and pattern ratio of hexagonal diameter-to-rib width  $\frac{D_{hex}}{W_{rb}}$  on the tensile modulus ratio  $\frac{E_{11}^*}{E_5}$  between the corrugated nanoplates and planar nanofilms obtained using the (a) analytical model and (b) FE model. (c) Optimal effect region (OER<sub>hex</sub>) for the corrugated nanoplates, which combines the bending stiffness enhancement factor BSEF<sub>hex</sub> and tensile stiffness reduction factor TSRF<sub>hex</sub>. (d) BSEF<sub>hex</sub>-to-TSRF<sub>hex</sub> ratio (the metamaterial figure of merit) for the corrugated nanoplates (L = 6 mm, W = 3 mm, t = 400 nm,  $W_{rib} = 10$  μm,  $h = 4 \sim 12$  μm, and  $D_{hex} = 80 \sim 120$  μm for all the cases).



**Fig. 5.** Optimal effect regions (OER<sub>pat</sub>) with respect to  $BSEF_{pat}$  and  $TSRF_{pat}$  for the corrugated nanoplates with the patterns of (a) rhombille with  $D_{rhom}=40\sim80~\mu\text{m}$ , (b) basketweave with  $D_{bask}=90\sim130~\mu\text{m}$  and (c) cylindrical with  $D_{cyl}=70\sim110~\mu\text{m}$  (L=6~mm, W=3~mm, t=400~nm,  $W_{pat}=10~\mu\text{m}$  and  $h=4\sim12~\mu\text{m}$  for all the cases).



**Fig. 6.** Areal density ratios  $\frac{AD_{pp}}{AD_{pf}}$  with respect to  $\frac{h}{t}$  and  $\frac{D_{pat}}{W_{pat}}$  for the nanoplates with the patterns of (a) hexagonal with  $D_{hex}=10\sim130~\mu\text{m}$ , (b) rhombille with  $D_{rhom}=10\sim290~\mu\text{m}$ , (c) basketweave with  $D_{bask}=10\sim170~\mu\text{m}$  and (d) cylindrical with  $D_{cyl}=10\sim210~\mu\text{m}$  (L=6~mm, W=3~mm, t=400~nm,  $W_{rib}=10~\mu\text{m}$ , and  $h=0.4\sim40~\mu\text{m}$  for all the cases). The shaded areas show the optimal effect regions (OER $_{pat}$ ) from Fig. 5.

and the nanofilms  $E_s$ . An analytical model was developed to fully characterize the tensile response of the corrugated nanoplates, and the predictions were validated with the experimental and numerical results, and satisfactory agreements were obtained. Architected nanoplates with rhombille, basketweave and cylindrical corrugations were also investigated theoretically; however, none of these patterns offered better performance than the honeycomb plates (i.e., achieving the optimal stiffness enhancements with the minimum weight). Together with our previous studies, we characterized the effects of corrugation patterns on the bending and tensile stiffnesses (i.e., bending stiffness strengthening and tensile stiffness reduction). Comparing with planar nanofilms that have the same overall geometries, the corrugation patterns enhanced the bending stiffness by at least 150 times ( $BSEF_{pat} > 150$ ) and decreased the tensile stiffness by at least 20 times ( $TSRF_{pat}$  < 0.05). More importantly, the systematic studies indicated that the geometry of the corrugated patterns can be used to tune the mechanical response over a large range. With this tunability, these proposed corrugated nanoplates can be employed for applications requiring light, rigid and flexible plates, e.g., wings of microflyers or expandable aerospace components that need to be deployed after take-off.

### **Declaration of competing interest**

The authors declare that they have no known competing financial interests or personal relationships that could have appeared to influence the work reported in this paper.

### Acknowledgments

This work was supported, in part, by the School of Engineering and Applied Science at the University of Pennsylvania, USA and a seed grant of the Center of Excellence for Materials Research and Innovation (CEMRI), National Science Foundation, USA grant DMR11-20901. This work was carried out in part at the Singh Center for Nanotechnology at the University of Pennsylvania, a member of the National Nanotechnology Coordinated Infrastructure (NNCI) network, which is supported by the National Science Foundation, USA (Grant No. ECCS-1542153). PJ acknowledges the Startup Fund of the Hundred Talent Program at the Zhejiang University. JC and WC were supported by the GAANN Fellowship from the US Department of Education, PKP acknowledges partial support from National Science Foundation, USA grant CMMI-1662101. The authors gratefully acknowledge the support of the staff of the Singh Center for Nanotechnology, Nanoscale Characterization Facility and Scanning and Local Probe facility, Materials Science & Engineering Instructional Laboratory at the University of Pennsylvania.

#### Appendix A. Supplementary data

Supplementary material related to this article can be found online at https://doi.org/10.1016/j.eml.2019.100599. See supplementary material for the detailed descriptions of corrugated nanoplates fabrication, Young's modulus calibration and tensile testing. Numerical and analytical modelings of the nanoplates subjected to tension were provided in detail as well. Systematic studies led to the discussions on the bending stiffness enhancement factor *BSEF* and tensile stiffness reduction factor *TSRF* 

#### References

- H.A. Atwater, A.R. Davoyan, O. Ilic, D. Jarwala, M.C. Sherrott, C.M. Went, W.S. Whitney, J. Wong, Materials challenges for the startshot lightsail, Nature Mater. 17 (2018) 861–867.
- [2] M. Lapine, D. Powell, M. Gorkunov, I. Shadrivov, R. Marques, Y. Kivshar, Structural tunability in metamaterials, Appl. Phys. Lett. 95 (2009) 084105.
- [3] M. Kadic, T. Buckmann, N. Stenger, M. Thiel, M. Wegener, On the practicability of pentamode mechanical metamaterials, Appl. Phys. Lett. 100 (2012) 191901.
- [4] A.A. Zadpoor, Mechanical metamaterials, Mater. Horiz. 3 (2016) 371.
- [5] C. Coulais, C. Kettenis, M. van Hecke, A characteristic length scale causes anomalous size effects and boundary programmability in mechanical metamaterials. Nat. Phys. 14 (2018) 40–45.
- [6] F. Fratemali, G. Carpentieri, A. Amendola, R.E. Skelton, V.F. Nesterenko, Multiscale tunability of solitary wave dynamics in tensegrity metamaterials, Appl. Phys. Lett. 105 (2014) 201903.
- [7] W. Lee, D.Y. Kang, J. Song, J.H. Moon, D. Kim, Controlled unusual stiffness of mechanical metamaterials, Sci. Rep. 6 (2016) 20312.
- [8] M.J. Mirzaali, R. Hedayati, P. Vena, L. Vergani, M. Strano, A.A. Zadpoor, Rational design of soft mechanical metamaterials: Independent tailoring of elastic properties with randomness, Appl. Phys. Lett. 111 (2017) 051903.
- [9] J. Bauer, J.R. Meza, T.A. Schaedler, R. Schwaiger, X. Zheng, L. Valdevit, Nanolattices: An emerging class of mechanical metamaterials, Adv. Mater. 29 (2017) 1701850.
- [10] S. Janbaz, M. McGuinness, A.A. Zadpoor, Multimaterial control of instability in soft mechanical metamaterials, Phys. Rev. Appl. 9 (2018) 064013.
- [11] A. Rafsanjani, A. Akbarzadeh, D. Pasini, Snapping mechanical metamaterials under tension, Adv. Mater. 27 (2015) 5931–5935.
- [12] H. Zhang, X. Guo, J. Wu, D. Fang, Y. Zhang, Soft mechanical metamaterials with unusual swelling behavior and tunable stress-strain curves, Sci. Adv. 4 (6) (2018) eaar8535.
- [13] Y. Jiang, Q. Wang, Highly-stretchable 3D-architected mechanical metamaterials, Sci. Rep. 6 (2016) 34147.
- [14] T. Frenzel, M. Kadic, M. Wegener, Three-dimensional mechanical metamaterials with a twist, Sci. 358 (2017) 1072–1074.
- [15] N. Hu, D. Chen, D. Wang, S. Huang, I, Trase, H.M. Grover, X. Yu, J.X.J. Zhang, Z. Chen, Stretchable kirigami polyvinylidene difluoride thin films for energy harvesting: design, analysis, and performance, Phys. Rev. Appl. 9 (2018) 021002.
- [16] A. Rafsanjani, K. Bertoldi, Buckling-induced kirigami, Phys. Rev. Lett. 118 (2017) 084301.
- [17] Y. Zhang, Z. Yan, K, Nan, D. Xiao, Y. Liu, H. Luan, H. Fu, X. Wang, Q. Yang, J. Wang, W. Ren, H. Si, F. Liu, L. Yang, H. Li, J. Wang, X. Guo, H. Luo, L. Wang, Y. Huang, J.A. Rogers, A mechanically driven form of kirigami as a route to 3D mesostructures in micro/nanomembranes, Proc. Natl. Acad. Sci. 112 (38) (2015) 11757–11764.
- [18] Y. Zhang, C.K. Lim, Z. Dai, G. Yu, J.W. Haus, H. Zhang, P.N. Prasad, Photonics and optoelectronics using nano-structured hybrid perovskite media and their optical cavities, Phys. Rep. 795 (2019) 1–51.
- [19] X. Jiang, S. Liu, W. Liang, S. Luo, Z. He, Y. Ge, H. Wang, R. Cao, F. Zhang, Q. Wen, J. Li, Q. Bao, D. Fan, H. Zhang, Broadband nonlinear photonics in few-layer MXene Ti3C2Tx (T=F, O, or OH), Laser Photo. Rev. 12 (2018) 1700229.

- [20] L. Lu, Z. Liang, L. Wu, Y. Chen, Y. Song, S.C. Dhanabalan, J.S. Ponraj, B. Dong, Y. Xiang, F. Xing, D. Fan, H. Zhang, Few-layer bismuthene: Sonochemical exfoliation, nonlinear optics and applications for ultrafast photonics with enhanced stability, Laser Photo. Rev. 12 (2018) 1700221.
- [21] K. Davami, L. Zhao, E. Lu, J. Cortes, C. Lin, D.E. Lilley, P.K. Purohit, I. Bargatin, Ultralight shape-recovering plate mechanical metamaterials, Nature Commun. 6 (2015) 10019.
- [22] C. Lin, S.M. Nicaise, D.E. Lilley, J. Cortes, P. Jiao, J. Singh, M. Azadi, G.G. Lopez, M. Metzler, P.K. Purohit, I. Bargatin, Nanocardboard as a nanoscale analog of hollow sandwich plates, Nature Commun. 9 (2018) 4442.
- [23] P. Jiao, W. Borchani, S. Soleimani, B. McGraw, Later-torsional buckling analysis of wood composite I-beams with sinusoidal corrugated web, Thin-Walled Struct. 119 (2017) 72–82.
- [24] P. Jiao, W. Borchani, H. Hasni, N. Lajnef, Static and dynamic post-buckling analyses of irregularly constrained beams under the small and large deformation assumptions, Int. J. Mech. Sci. 124 (2017) 203–215.
- [25] W. Borchani, P. Jiao, R. Burgueno, N. Lajnef, Control of postbuckling mode transitions using assemblies of axially loaded bilaterally constrained beams, J. Eng. Mech. 143 (10) (2017) 04017116.
- [26] S. Yang, P. Liu, M. Yang, Q. Wang, J. Song, L. Dong, From flexible and stretchable meta-atom to metamaterial: A wearable microwave meta-skin with tunable frequency selective and cloaking effects, Sci. Rep. 6 (2016) 21921.
- [27] Z. Liu, X. Yan, M. Qi, Y. Zhu, D. Huang, X. Zhang, L. Lin, Artificial insect wings with biomimetic wing morphology and mechanical properties, Bioinspir & Biomime. (2017) http://dx.doi.org/10.1088/1748-3190/aa7f16.
- [28] B. Singh, I. Chopra, Insect-based hover-capable flapping wings for micro air vehicles: Experiments and analysis, AIAA J. 46 (9) (2008) 2115–2135.
- [29] P. Jiao, S.M. Nicaise, C. Lin, P.K. Purohit, I. Bargatin, Extremely sharp bending and recoverability of nanoscale plates with honeycomb corrugation, Phys. Rev. Appl. 11 (2019) 034055.
- [30] H. Tao, L.R. Chieffo, M.A. Brenckle, S.M. Siebert, M. Liu, A.C. Strikwerda, K. Fan, D.L. Kaplan, X. Zhang, R.D. Averitt, F.G. Omenetto, Metamaterials on paper as a sensing platform, Adv. Mater. 23 (2011) 3197–3201.
- [31] H.U. Chung, B.H. Kim, J.Y. Lee, J. Lee, Z. Xie, E.M. Ibler, K.H. Lee, A. Banks, J.Y. Jeong, J. Kim, C. Ogle, D. Grande, Y. Hu, H. Jang, P. Assem, D. Ryu, J.W. Kwak, M. Namkoong, J.B. Park, Y. Lee, D.H. Kim, A. Ryu, J. Jeong, K.I. Jang, J. Kim, Y. Zhang, R. Ghaffari, C.M. Rand, M. Schau, A. Hamvas, D.E. Weese-Mayer, Y. Huang, S.M. Lee, C.H. Lee, N.R. Shanbhag, A.S. Paller, S. Xu, J.A. Rogers, Binodal, wireless epidermal electronic systems with in-sensor analytics for neonatal intensive care, Sci. 363 (2019) 947.
- [32] F. Scarpa, S. Adhikari, A.S. Phani, Effective elastic mechanical properties of single layer graphene sheets, Nanotechnology 20 (2009) 065709.
- [33] E. Akturk, O.U. A.K.turk, S. Ciraci, Single and bilayer bismuthine: Stability at high temperature and mechanical and electronic properties, Phys. Rev. B 94 (2016) 014115.
- [34] U. Yorulmaz, A. Ozden, N.K. Perkgoz, F. Ay, C. Sevik, Vibrational and mechanical properties of single layer mxene structures: a first-principles investigation, Nanotechnology 27 (2016) 335702.
- [35] K. Javed, W.J. Li, S.S. Ali, D.W. Shi, U. Khan, S. Riaz, X.F. Han, Enhanced exchange bias and improved ferromagnetic properties in Permalloy-BiFe0.95Co0.05O3 core-shell nanostructures, Sci. Rep. 5 (2015) 19302
- [36] L.J. Gibson, M.F. Ashby, Cellular Solids: Structure and Properties, second ed., Cambridge University Press, ISBN: 0 521 499119, 1997.